

# Physics issues in simulations with dynamical overlap fermions

Thomas DeGrand and Stefan Schaefer

*Department of Physics, University of Colorado, Boulder, CO 80309 USA*

We discuss the impact of various improvements on simulations of dynamical overlap fermions using the Hybrid Monte Carlo algorithm. We focus on the usage of fat links and multiple pseudo fermion fields.

## I. INTRODUCTION

As lattice simulations of QCD push to ever smaller quark masses, they increasingly benefit from discretizations which respect chiral symmetry. Simulations with  $N_f$  flavors of degenerate overlap [1, 2] fermions encode an exact  $SU(N_f) \otimes SU(N_f)$  chiral symmetry, and are the cleanest theoretical description of lattice fermions known to date. They have several theoretical advantages as compared to the traditional formulations using Wilson or staggered quarks. Their correct implementation of chiral symmetry protects them from exceptional configurations which plague simulations with Wilson fermions. Staggered fermions have a  $U(1) \otimes U(1)$  chiral symmetry, and are probably the easiest fermions to simulate, but one staggered fermion flavor corresponds to four continuum “tastes.” It is unknown whether the standard trick of performing staggered simulations by taking the quarter root of the fermion determinant is justifiable. Staggered fermions also have a complicated low energy effective field theory due to taste-breaking interactions, while the low energy dynamics of overlap fermions is basically identical to that of the continuum. Domain wall fermions involve simulations on a five-dimensional background. Flavor symmetry is unbroken, and chiral symmetry becomes exact as the length of the fifth dimension goes to infinity. Recent large scale simulations with domain wall fermions claim to have good chiral behavior[3]. However, a paper[4] which appeared nearly simultaneously, describing requirements for good chiral behavior for matrix elements appropriate to CP violation in kaons, set somewhat more stringent requirements than the simulation claimed. We prefer to avoid these questions by working from the beginning with exact chiral symmetry for dynamical fermions.

Unfortunately, the much higher cost of applying the Dirac operator on a vector prevents us from using overlap fermions in large scale simulations. Until now only exploratory studies have been published [5, 6, 7]. This paper is also only exploratory. Its goal is to investigate several methods to improve the performance of the Hybrid Monte Carlo (HMC) algorithm [8] and the extension proposed in [6] for these fermions. The major new ingredient is the use of a differentiable fat link, the “stout link” of Peardon and Morningstar[9], as the gauge connection for the fermions. Fat links are well known to reduce the computational cost of overlap fermions [10, 11]. Their bottleneck has been that the existing forms could not be used in the standard dynamical fermion updating algorithm, Hybrid Monte Carlo. Stout links overcome that difficulty and give a speedup of about an order of magnitude in computer time compared to simulations of overlap fermions with thin links.

The eigenvalues of the overlap Dirac operator lie on a circle in the complex plane. The overlap operator maps the eigenvalues of a “kernel” action onto this circle. The eigenmodes of these free kernel actions typically lie on arcs, and the eigenvalues of the kernel in an arbitrary background gauge field can be dense everywhere. Fat links tend to force the eigenvalues back onto the free-field arcs, reducing the density of eigenmodes near the center of the overlap circle. Golterman and Shamir[12] have recently suggested that chiral symmetry for overlap action could be realized differently if the eigenmodes of the kernel whose eigenvalues lie near the center of the circle become delocalized in space. By reducing the density of eigenmodes, we reduce the probability that nearly degenerate modes exist and can mix. We will show that fat link kernel eigenmodes are more localized than thin link kernel eigenmodes.

The major difference between dynamical simulations of overlap fermions and other kinds is the discontinuity in the overlap fermionic action associated with changing the topological sector. If carefully treated, away from these topological boundaries, the overlap fermion force in Hybrid Monte Carlo is never singular, and so a larger integration step size can be tolerated. For us, the force due to the gauge part of the action is actually larger than the fermion force. This part of the force is inexpensive to compute, and it can be easily smoothed by using the Sexton-Weingarten[13] multi-scale time-step update.

At a topological boundary, the step in the fermionic action can be treated by the algorithm proposed in [6] which reflects or refracts the momentum at the discontinuity in the fermionic action in analogy to classical mechanics. Pseudo-fermions give only a noisy estimator of the fermion action. The noise suppresses topological changes. This problem can be partially ameliorated with the multi-pseudofermion method of Hasenbusch[14, 15].

The use of improved actions is accompanied by the necessity of choosing values for a large parameter set – nearly all of which are related to coefficients of (formally) irrelevant operators. This is only psychologically different from the use of more standard actions, where essentially all these parameters are set to zero value and ignored. Generally, there is a wide latitude in the choice of these parameters. As we proceed, we will discuss our choices (summarizing

everything in the conclusion), with a description of what will happen when the parameters are varied, when it is available. We cannot imagine that anyone would want to do simulations with precisely our choice of parameters, but we believe that any reasonably similar action would produce similar results.

## II. ACTION AND ALGORITHM

### A. Definitions

To fix the conventions, let us recall the definition of the overlap Dirac operator  $D_{\text{ov}}(m_q)$ . It is constructed from some lattice Dirac operator (in the following called the kernel operator)  $d(\mu)$  and its associated Hermitian Dirac operator  $h(\mu) = \gamma_5 d(\mu)$  with mass term  $\mu$ . The massless Hermitian overlap operator  $H(0) = \gamma_5 D_{\text{ov}}(0)$  is defined as

$$H(0) = R_0 [\gamma_5 + \epsilon(h(-R_0))] \quad (1)$$

with  $R_0 > 0$  the radius of the Ginsparg–Wilson[16] circle. The matrix sign function  $\epsilon(h)$  can be defined by

$$\epsilon(h) = \frac{h}{\sqrt{h^2}} = \sum_{\lambda} \text{sign}(\lambda) |\lambda\rangle\langle\lambda| \quad (2)$$

with  $\lambda$  the eigenvalues and  $|\lambda\rangle$  the eigenvectors of  $h(-R_0)$ . (Whenever no argument of  $h$  is given,  $h(-R_0)$  is implied.) The massive overlap Dirac operator is

$$D(m) = (1 - \frac{m}{2R_0})D(0) + m, \quad (3)$$

and the square of the massive Hermitian overlap operator  $H(m)$  can then be written as

$$H(m)^2 = (1 - \frac{m^2}{4R_0^2})H(0)^2 + m^2 \quad (4)$$

with

$$H^2(0) = R_0^2 [2 + \gamma_5 \epsilon(h(-R_0)) + \epsilon(h(-R_0))\gamma_5] . \quad (5)$$

Since  $[H^2(m), \gamma_5] = 0$ ,  $H^2$  can be written as a sum of two operators each of which acts only on one chiral sector,  $H^2 = H_+^2 + H_-^2$ . In a sector with topological charge  $Q$ ,  $H^2(0)$  has, assuming the correctness of the vanishing theorem,  $|Q|$  zero modes of chirality  $\sigma = \text{sign}(Q)$  and  $|Q|$  eigenmodes with eigenvalue  $4R_0^2$  in the opposite chirality. The spectra of  $H_+(0)^2$  and  $H_-(0)^2$  outside of eigenvalues at  $\lambda = 0, 4R_0^2$  are identical. Changing the topological sector therefore amounts to transforming a pair of eigenvalues with opposite chirality and eigenvalues  $\lambda$  to eigenvalues 0 and  $4R_0^2$ , i.e. a non-continuous change of the spectrum. The rest of the spectrum will also change significantly. This will become important in the discussion of the rate at which the topological sector changes.

We will construct the sign function  $\epsilon(h(-R_0))$  by projecting out the lowest  $n_{\text{eig}}$  eigenmodes  $|\lambda\rangle$  of the kernel operator (with respect to modulus) and using a Zolotarev approximation of order  $n_z$  for the rest of the spectrum [17, 18],

$$\epsilon(h) = \sum_{\lambda} \text{sign}(\lambda) P_{\lambda} + \sum_{i=1}^{n_z} h \frac{b_i}{h^2 + c_i} (1 - \sum_{\lambda} P_{\lambda}), \quad (6)$$

with  $P_{\lambda} = |\lambda\rangle\langle\lambda|$  the projector on the eigenstate  $|\lambda\rangle$ . We fix  $n_z$ ,  $b_i$  and  $c_i$  such that the precision of the sign function between at least  $\lambda_{n_{\text{eig}}}$  and the maximal retained eigenvalue of the kernel is better than some given value, e.g.  $10^{-7}$ .

The action of the sign function on a vector  $\phi$  is computed by using a multi-mass [19] conjugate gradient (CG) to invert  $h^2 + c_i$ , after projecting out the eigenmodes of the kernel operator from the vector. We will refer to this as the inner CG as opposed to the outer CG used to invert  $H^2(m)$ . We calculate the eigenmodes by the conjugate gradient method of Ref. [20]. We choose an accuracy for the step function and monitor the norm of the vector  $\epsilon(h)\phi$  during the CG iteration, stopping when either the the observed accuracy of the step function is achieved, or when the inner CG converges. (Of course, we wish to set the accuracy of the inner CG high enough, that the second result never happens.)

As proposed in Ref. [21] we adjust the accuracy of the inner CG,  $r_{\text{in}}$ , depending on the current residue of the outer CG  $r_{\text{out}}$  according to

$$r_{\text{in}} = \min(r_0 \frac{|b|}{r_{\text{out}}}, r_{\text{cut}}) \quad (7)$$

with  $b$  the source vector of the inversion,  $r_0$  the target residue and  $r_{\text{cut}}$  a maximal inner residue. Since we want to make sure that this does not introduce an additional inaccuracy we restart the CG after convergence with the inner residue fixed to  $r_0$ . With a good choice for  $r_{\text{cut}}$  fewer inner CG steps will be needed in the first pass and the restarted CG will converge in 1-2 steps.

## B. The kernel operator

The choice of the kernel Dirac operator used in the construction of the overlap provides an opportunity of optimization. Most groups use the Wilson operator because of the low computational effort to apply it on a vector. One might also choose an operator which almost fulfills the Ginsparg-Wilson relation like the hyper-cubic actions proposed in Refs. [22, 23] and tested in [24]. This has the advantage that the number of operations to ‘transform’ this operator into the overlap operator is low, e.g. it takes a small number of inner CG steps. However, the application of the kernel operator alone is much more expensive than for the Wilson action, involves more communication, and the fermionic force is cumbersome to code. We wish to find an optimum in between these two approaches. The application of the operator should be as cheap as possible with respect to computation and communication. But it also should approximate the Ginsparg-Wilson circle in some way.

The optimization has two parts: the choice of a free field action and the choice of a gauge connection.

We use an action similar to the one studied in Ref. [10] which has nearest and diagonal neighbor interactions. To be precise let us parameterize the associated massless free action by

$$S = \sum_{x,r} \bar{\psi}(x) [\eta(r) + i\gamma_\mu \rho_\mu(r)] \psi(x+r) \quad (8)$$

with  $r$  connecting nearest neighbors ( $\vec{r} = \pm\hat{\mu}$ ;  $\eta = \eta_1$ ,  $\rho_\mu = \rho_1$ ) and diagonal neighbors ( $\vec{r} = \pm\hat{\mu} \pm \hat{\nu}$ ,  $\nu \neq \mu$ ;  $\eta = \eta_2$ ,  $\rho_\mu = \rho_\nu = \rho_2$ ). The constraint  $\eta(r=0) = \eta_0 = -8\eta_1 - 24\eta_2$  enforces masslessness on the spectrum, and  $-1 = 2\rho_1 + 12\rho_2$  normalizes the action to  $-\bar{\psi}i\gamma_\mu\partial_\mu\psi$  in the naive continuum limit. Thus there are three free parameters to choose. These three parameters can be reduced to one by requiring that each of the couplings of a fermion to its neighbors is a projector, proportional to  $1 \pm \hat{n} \cdot \gamma$ . This is a familiar trick for Wilson action simulations. There, one gains almost a factor of two in speed from the trick because the multiplication of the gauge connection times the spinor only needs to be done on two, not four Dirac components, and because the ‘gather’ of a spinor on a neighboring site does not need all four Dirac components, only the linear combination of two components which participates in the projection. For nearest neighbors, a projector action corresponds to the constraint  $\eta_1 = \rho_1$  (up to signs) and for the diagonal neighbors,  $\eta_2 = \sqrt{2}\rho_2$ . With this action, the gain in speed on a single-node computer is only about 8-10 per cent, since the diagonal projection itself has an overhead. Of course, on a parallel machine, projection halves the necessary internodal communication.

The action we use in the simulations presented in this paper uses  $\rho_1 = -1/6$  and  $\rho_2 = -1/18$ . We also add a clover term with the tree-level clover coefficient appropriate to this action of 1.278. For these parameters it seems optimal to set the radius of the Ginsparg-Wilson circle  $R_0$  to 1.2 since it is closest to the behavior of the kernel for the low-lying eigenmodes. We tested this value by timing a quenched approximation calculation of eigenmodes, for various  $R_0$  values. This was done with Wilson action gauge fields, at coupling  $\beta = 5.9$ , or a lattice spacing of about 0.13 fm. One could vary  $R_0$  by  $\pm 0.2$  without much effect. In Fig. 1 we show the free field spectrum of the kernel Dirac operator we use together with several Ginsparg-Wilson circles. Let us remark that contrary to the Wilson operator, which has a maximal eigenvalue at 16, this operator has it at about 4. This alone reduces the condition number  $\kappa = \lambda_{\text{max}}/\lambda_{\text{min}}$  of the  $h^2$ , which controls the convergence of the inner CG, by a factor of about 16.

The other ingredient of our kernel action, the stout link as a gauge connection, is so important that it deserves a separate discussion below, in Sec. IV.

## C. Hybrid Monte Carlo

We consider simulations with two flavors of degenerate-mass fermions. In a completely standard approach, we add to the gauge action a set of momenta  $\pi_\mu(n)$  (with total energy  $\frac{1}{2} \sum_{\mu,n} \pi_\mu(n)^2$ ). To include the fermions, we introduce their action using pseudo-fermions

$$S_f[U, \phi^\dagger, \phi] = \phi^\dagger H(m)^{-2} \phi \quad (9)$$

where the pseudo-fermion fields  $\phi$  are a set of four-component spinors. At the beginning of each trajectory we perform a heat-bath initialization of the fermion action by casting a vector of four-component colored Gaussian random numbers  $R$  and initialize  $\phi = HR$ .

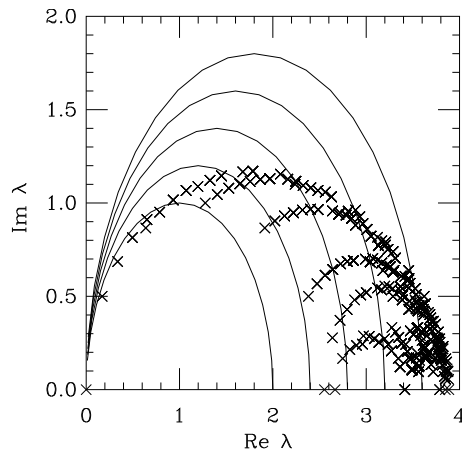


FIG. 1: Eigenmode spectrum of the kernel action used in this work on a finite lattice, with superimposed circles (which show the spectrum of overlap actions). The five circles have radius 1.0, 1.2, 1.4, 1.6, 1.8.

We want to study the effect of additional pseudo-fermion fields as advocated in Refs. [14, 15] on the performance of the HMC algorithm. One therefore rewrites the fermion determinant of two degenerate fermions as

$$\det H^2(m) = \det H^2(m_{N_p}) \prod_{i=1}^{N_p-1} \det \frac{H^2(m_i)}{H^2(m_{i+1})} \quad (10)$$

with  $m_1 = m$  and  $m_i < m_{i+1}$  with suitably chosen larger masses. Using pseudo-fermions  $\phi_i$  to deal with the determinants, this leads as usual to the effective action

$$S_{\text{eff}}[U, \phi_i^+, \phi_i] = S_g[U] + S_f[U, \phi_i^+, \phi_i] \quad (11)$$

with  $S_g[U]$  the gauge action and

$$S_f[U, \phi_i^+, \phi_i] = \phi_0^+ H^{-2}(m_{N_p}) \phi_0 + \sum_{j=1}^{N_p-1} \phi_j^+ \frac{H^2(m_{j+1})}{H^2(m_j)} \phi_j. \quad (12)$$

To calculate the fermion force one has to know the variation of the fermion action. Since  $[H^2, \gamma_5] = 0$  one can split the fermionic action into two contributions of definite chirality. In the following we restrict ourselves to one pseudo-fermion field. The generalization to multiple fields is trivial. For a chiral source  $\phi$  with chirality  $\sigma = \pm 1$  we follow [8] and [5] and compute the simulation time derivative of the fermionic action

$$\frac{d}{d\tau} S_f[U, \phi^+, \phi] = \phi^+ \frac{d}{d\tau} H^{-2} \phi = -2(R_0^2 - \frac{m^2}{4}) \sigma \psi^+ \frac{d}{d\tau} \epsilon(h) \psi \quad (13)$$

with  $\psi = H^{-2} \phi$ . This is only valid as long as no eigenvalue of  $h(-R_0)$  is zero. Since an eigenvalue changing sign causes a step in the action, we get an additional contribution

$$\frac{d}{d\tau} S_f[U, \phi^+, \phi] \Big|_{\text{disc}} = \delta(\lambda) \Delta S_f[U] \lambda. \quad (14)$$

It is very difficult to approximate the derivative of the step function by the derivative of its Zolotarev approximation, because near topological boundaries eigenmodes of  $h$  will develop arbitrarily small eigenvalues. In order to compute the variation of the approximation to the sign function Eq. (6), we have to know the variation of the projectors. This can be taken into account by using first order perturbation theory [25],

$$\delta P_\lambda = \frac{1}{\lambda - h} (1 - P_\lambda) \delta h P_\lambda + P_\lambda \delta h^+ \frac{1}{\lambda - h} (1 - P_\lambda). \quad (15)$$

The derivative of the approximation of the sign function used in Eq. (13) thus becomes

$$\psi^+ \frac{d}{d\tau} \epsilon(h) \psi = \psi^+ (1 - P) \frac{d}{d\tau} \tilde{\epsilon}(h) (1 - P) \psi + \sum_{\lambda} \left\{ -\chi_{\lambda}^+ \dot{h} \tilde{\rho}_{\lambda} - \tilde{\rho}_{\lambda}^+ \dot{h} \chi_{\lambda} + \epsilon(\lambda) (\rho_{\lambda}^+ \dot{h} \tilde{\rho}_{\lambda} + \tilde{\rho}_{\lambda}^+ \dot{h} \rho_{\lambda}) \right\} \quad (16)$$

with  $P = \sum_{\lambda} P_{\lambda}$  and  $\tilde{\epsilon}(h)$  the Zolotarev approximation to the sign function. The  $\chi$  and  $\rho$  are defined as

$$\rho_{\lambda} = \frac{1}{\lambda - h} (1 - P_{\lambda}) \psi ; \quad \tilde{\rho}_{\lambda} = P_{\lambda} \psi ; \quad \chi_{\lambda} = \frac{1}{\lambda - h} \epsilon(h) (1 - P) \psi . \quad (17)$$

The derivative of the Zolotarev approximation can be simplified to

$$\frac{d}{d\tau} \sum_l h \frac{b_l}{h^2 + c_l} = \sum_l \frac{1}{h^2 + c_l} [c_l b_l \dot{h} - b_l h \dot{h} h] \frac{1}{h^2 + c_l} . \quad (18)$$

The term in Eq. (14) comes from the derivative of the step function at  $\lambda = 0$  where the height of the step in the fermionic action is  $\Delta S_f$ . For this term we use now the Feynman-Hellmann theorem

$$\dot{\lambda} = \chi^+ \dot{h} \chi \quad (19)$$

with  $\chi$  the zero-mode of the kernel operator  $h$ . This force acts only if the eigenvalue  $\lambda$  of the kernel operator  $h(-R_0)$  changes sign. At these points the topology changes, because using Eqs. (1) and (2)

$$Q = \text{Tr} H_{\text{ov}} = \sum_{\lambda} \text{sign}(\lambda) . \quad (20)$$

To compute the height of this step in the action, we evolve the gauge fields in simulation time onto the  $\lambda = 0$  surface. Then we compute  $S_f$  on both sides of the surface, where we just change the sign of the value of the crossing eigenmode. This is the only source of discontinuity. Anything else which might change across this surface does so continuously and is thus captured by the equations of motion. Then we use the prescription of Ref. [6] to alter the momentum  $\pi$  depending on whether the step in potential  $\Delta S_f$  is high enough to reflect at the surface or whether one can refract into the other topological sector. The new momenta then are

$$\Delta \pi = \begin{cases} -N \langle N | \pi \rangle + N \text{sign} \langle N | \pi \rangle \sqrt{\langle N | \pi \rangle^2 - 2\Delta S_f} & \text{if } \langle N | \pi \rangle^2 > 2\Delta S_f \\ -2N \langle N | \pi \rangle & \text{if } \langle N | \pi \rangle^2 \leq 2\Delta S_f \end{cases} \quad (21)$$

where  $\Delta S_f$  is the height of the discontinuity,  $N$  the vector normal to the surface of zero eigenvalue and  $\pi$  the molecular dynamics momenta. The scalar product is defined by

$$\langle N | \pi \rangle = \sum_x \text{Tr}(N^+ \pi) . \quad (22)$$

Using Eq. (19), the normal vector  $N$  is computed using the derivative of the kernel action with respect to  $U$

$$N(x, \mu) = \left[ U(x, \mu) \langle \chi | \frac{\delta h}{\delta U(x, \mu)} | \chi \rangle \right]_{\text{TA}} . \quad (23)$$

with  $|\chi\rangle$  the zero-mode of the kernel operator and we take the traceless anti-Hermitian part so that  $\pi$  itself stays traceless and anti-Hermitian.

A word on the evaluation of  $\rho_{\lambda}$ : Since  $\lambda$  is an eigenvalue of  $h$ , the matrix  $1/(\lambda - h)$  is singular. Although  $1/(\lambda - h)(1 - P_{\lambda})$  is well defined, in a numerical calculation  $\lambda$  and  $|\lambda\rangle$  may not be sufficiently accurately known for the inversion to be stable. In our simulation we therefore compute  $1/(\lambda + \delta_i - h)(1 - P_{\lambda})\psi$  for several  $\delta_i$  and interpolate to  $\delta = 0$  afterward.

In our simulation the kernel operator is constructed from stout links. Thus, after calculating the variation of the kernel operator  $\delta h$  with respect to the stout links one has to apply the chain rule as described in Ref. [9] to get the variation with respect to the unsmear link variable  $U(x, \mu)$ .

In order to maintain a high acceptance rate, it is crucial to monitor whether a mode has crossed the zero eigenvalue surface. Fortunately, functions of the gauge field variables, including eigenmodes of the kernel, evolve slowly in simulation time. The identification of the modes before and after a molecular dynamics time step is done by computing their scalar products. If the product of the vector at the beginning of the step with one at the end has an absolute

value close to one, the two modes are identified. A technical problem occurs if the modes become degenerate during the time step since the wave functions can mix in this case. However, enough similarity remains to identify the pair of the two modes which have mixed. If we have identified that at least the eigenvalue of one mode has changed sign we use the van Wijngaarden-Dekker-Brent method [26] to find the first point in simulation time where an eigenvalue vanishes.

To integrate the equations of motion we employ a Sexton-Weingarten scheme [13] setting the time-scale of the gauge updates to  $1/n_{SW}$  of the scale for the fermionic updates  $\delta\tau$ . Using the following notation for the updates

$$\begin{aligned} T_{PG}(\tau) &: \pi \rightarrow \pi - i\tau\delta_U S_g[U] \\ T_{PF}(\tau) &: \pi \rightarrow \pi - i\tau\delta_U S_f[U] \\ T_U(\tau) &: U \rightarrow e^{i\tau\pi}U \end{aligned} \quad (24)$$

the updating algorithm is composed of the following elementary steps:

- 1) Update momenta with fermion force:

$$\pi \rightarrow T_{PF}(\delta\tau/2)\pi \quad (25)$$

- 2) Update gauge fields: Do  $n_{SW}$  steps of the gauge update:

$$U \rightarrow [T_{PG}(\delta\tau/(2n_{SW}))T_U(\delta\tau/n_{SW})T_{PG}(\delta\tau/(2n_{SW}))]^{n_{SW}} \quad (26)$$

- 3) Calculate eigenmodes of the kernel operator, decide whether an eigenmode has changed sign. If this is the case go to the time when this has happened, change the momenta according to Eq. (21) and evolve until the end of the time step.

- 4) Update momenta with fermion force.

$$\pi \rightarrow T_{PF}(\delta\tau/2)\pi \quad (27)$$

### III. SIMULATION PARAMETERS

We wanted to test the algorithm at parameters appropriate to simulations which could be used to do physics. Quenched overlap simulations become increasingly difficult as the gauge coupling is carried into the strong coupling regime, as the cost of the inner CG grows. We also fear encountering the region of the Golterman-Shamir vanishing mobility edge[12]. Thus, the largest lattice spacing  $a$  which we feel we can tolerate is at about  $a = 1/(6T_c)$  or about 0.2 fm at a nominal  $N_f = 2$  deconfinement temperature of 150 MeV. For our first round of tests, we do not need an accurate determination of  $a$ . Accordingly, we equilibrated  $6^4$  volumes at parameter values near their values for deconfinement. The crossover from the confined phase will be very rounded, and the deconfinement phase will not be very physical, since Polyakov loops in all directions will order, but we will still have a rough idea of the lattice spacing. After the simulation parameters are optimized, we can go to bigger spatial volumes.

We simulated using the Lüscher-Weisz gauge action [27]. We approximated the tadpole improved coefficients of Ref. [28]. Explicitly the action reads

$$S[U] = \beta_1 \sum_{pl} \frac{1}{3} \text{Re Tr} [1 - U_{pl}] + \beta_2 \sum_{rt} \frac{1}{3} \text{Re Tr} [1 - U_{rt}] + \beta_3 \sum_{pg} \frac{1}{3} \text{Re Tr} [1 - U_{pg}], \quad (28)$$

$$\beta_2 = -\frac{\beta_1}{20 u_0^2} [1 + 0.4805 \alpha], \quad \beta_3 = -\frac{\beta_1}{u_0^2} 0.03325 \alpha, \quad (29)$$

with  $U_{pl}$  the plaquette,  $U_{rt}$  the  $1 \times 2$  rectangle, and  $U_{pg}$  the perimeter-6 ‘‘parallelogram’’ loop, and

$$u_0 = \left(\frac{1}{3} \text{Re Tr} \langle U_{pl} \rangle\right)^{1/4}, \quad \alpha = -\frac{\ln\left(\frac{1}{3} \text{Re Tr} \langle U_{pl} \rangle\right)}{3.06839}. \quad (30)$$

After running on  $6^4$  lattices using about 200 trajectories we measured  $u_0 = 0.86$  for several parameter sets, with little variation. We therefore decided to set  $u_0 = 0.86$  for all our production runs. Even though this is only a rough

estimate and not a self consistent determination of  $u_0$ , we expect this to capture most of the effect of the tadpole improvement.

In nearly all runs we applied two levels of isotropic stout smearing and chose the smearing parameter  $\rho = 0.15$ , see Sec. IV. This value was determined by maximizing the average value of the plaquette constructed from the fat links on a number of quenched configurations. This is the same strategy as used in Ref. [29] to determine the parameters of HYP smearing. We believe that any value in the range between 0.1 and 0.2 would work nearly as well.

We performed runs at bare quark masses  $am_q = 0.05, 0.1$  at  $\beta$  values such that we ran at both sides of the (pseudo) phase transition. A plot of the plaquette vs. gauge coupling  $\beta$  is shown in Fig. 2. In order to illustrate the change in the Polyakov loop as a function of  $\beta$  we show a scatter plot at  $am_q = 0.1$  in Fig. 3.

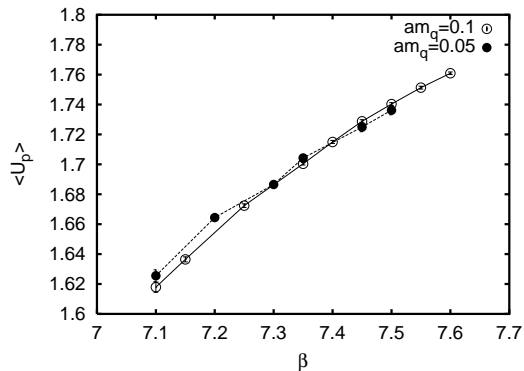


FIG. 2: Plaquette vs gauge coupling  $\beta = 10/g^2$  from dynamical overlap simulations on  $6^4$  lattices with quark masses  $am = 0.05$  and  $0.1$ .

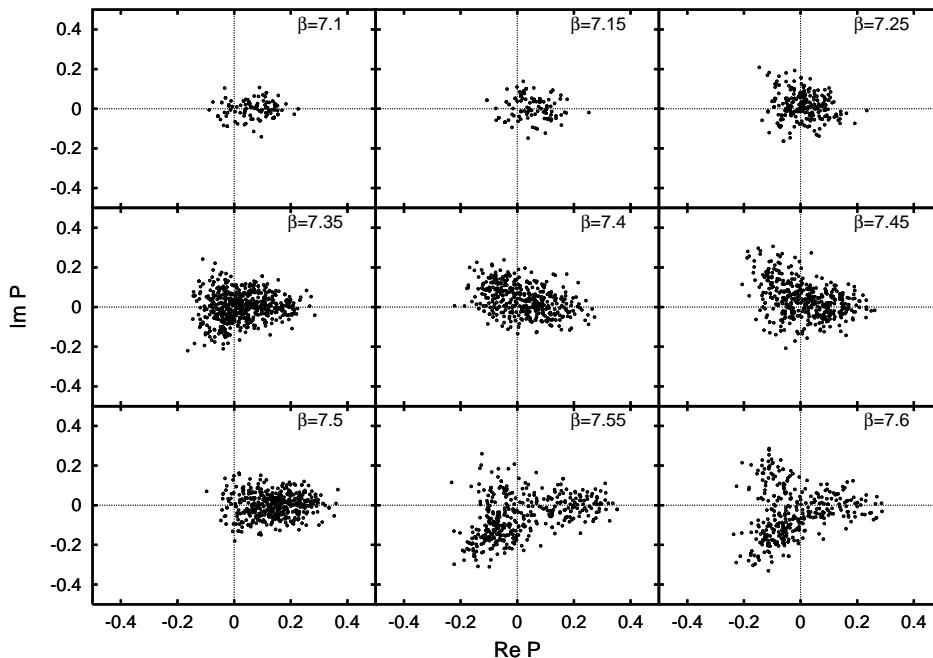


FIG. 3: Scatter plot of the Polyakov loop with quark masses  $am = 0.1$  on the  $6^4$  lattices for various values of  $\beta$ .

We set the precision of the step function to be  $10^{-7}$  and ran the CG for the fermionic action to a residue of  $10^{-6}$ . For the HMC algorithm we chose to set the number of gauge update steps  $n_{SW} = 12$  since this provided us with a gauge force of roughly the same size as the fermion force. Due to the high cost of the fermion inversions the gauge updates are still a negligible fraction of the cost the whole update.

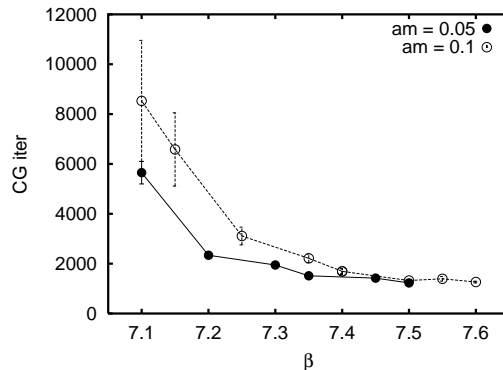


FIG. 4: Number of applications of the kernel operator on a vector per step and pseudo-fermion field as a function of the gauge coupling. The runs at  $am_q = 0.05$  were done with 2 pseudo-fermions, the runs at  $am_q = 0.1$  with three.

A trajectory of molecular dynamics evolution had a typical time step of  $\delta t = 1/20$  for  $am_q = 0.05$  and  $\delta t = 1/15$  for  $am_q = 0.1$ . At each step we computed  $n_{\text{eig}} = 8$  eigenmodes of the kernel operator. The cost of these eigenmodes is 5%–10% overhead in the confined phase and rises to as large as 50% at high  $\beta$  where the inversion is much cheaper. One has to make sure that the gauge field moves between two computations of the eigenvalues only such that an eigenvalue which has changed sign is among the  $n$  modes before and after the elementary step. This along with the requirement that preferably not more than one eigenmode changes sign per elementary step are the limiting requirements to the step size.

We ran simulations on our array of 31 old 800 Mhz P-III's and 12 new 3.2 Ghz P-IVE's, all in single-processor mode. At  $\beta = 7.35$  and  $am_q = 0.1$  we collect approximately 40 trajectories per day on the newer machines. Fig. 4 gives the dependence on the gauge coupling of the number of applications for the kernel operator on a vector per elementary step and pseudo-fermion field. Our code is based on the MILC package[30], with SSE routines[31] for all  $SU(3)$  matrix multiplication.

We now describe explorations of various parameter choices.

First, there are some small tricks. We always begin the outer CG for the fermionic force with trial vectors taken by interpolating solutions from the previous two time steps. We also extrapolate the identified eigenvectors of  $h$  to begin the Conjugate Gradient calculation of new eigenmodes. Careful tuning of the  $r_{\text{cut}}$  parameter (recall Eq. 7) can reduce the number of inner CG steps (this from a  $\beta = 7.2$ ,  $m = 0.05$ ,  $\delta\tau = 1/20$  run) from about 35 to about 20.

Fig. 5 illustrates the effect of Sexton-Weingarten updating. We plot the average over  $e^{\Delta E}$  ( $\Delta E$  being the energy violation after one molecular dynamics trajectory of length 1) which governs the acceptance probability. It is from a run with  $\beta = 7.4$  and  $am_q = 0.1$  with time-step  $\delta\tau = 1/15$ . We started from the same equilibrium configuration and average over 19 trajectories. We see a considerable reduction in energy non-conservation as  $n_{SW}$  increases. In this run, we can compare the fermion force per direction  $\sqrt{\sum_x \text{Tr} F_\mu^+(x) F_\mu(x)}$  to the gauge force: the gauge force is about an order of magnitude larger. So setting  $n_{SW} \simeq 12$  reduces the gauge impulse to roughly the level of the fermion impulse.

This factor of 10 falls to about a factor of five in thin link simulations: the fermion force doubles. This probably happens because thin link fermions do not decouple from high-momentum gluon modes. A glance at a time history of  $\Delta E$  shows Sexton-Weingarten updating works less well; one would simply have to lower the molecular dynamics time step  $\delta\tau$  to reduce energy violation.

We typically run with either  $N_p = 2$  or 3 pseudo-fermion fields. As we are going to discuss in Sec. V, this increases the number of changes of topology significantly whereas it has no impact on the step size. In order to check the implementation of the additional pseudo-fermions we compared the plaquette for  $N_p = 1, 2$  and 3 fields. They agreed within statistical errors.

#### IV. IMPACT OF FAT LINKS

It has been long known that fat links can significantly decrease the computational cost of applying the overlap operator on a vector [11]. They also have a beneficial effect on the locality of the overlap operator [32]. Recently stout smearing [9], which is analytic in the gauge fields and thus suitable for the HMC algorithm, has become available.



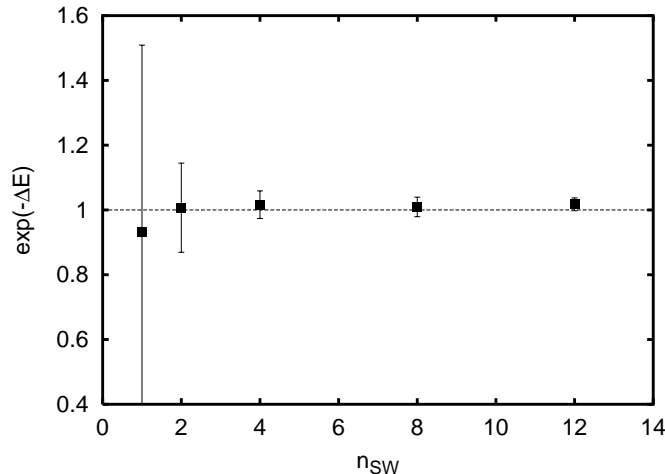


FIG. 5: The average acceptance probability  $e^{\Delta E}$  with  $\Delta E$  the violation in the microcanonical energy as a function of the number of Sexton-Weingarten steps  $n_{SW}$ . We average over 19 trajectories which started from the same equilibrium configuration at  $\beta = 7.4$  and  $am_q = 0.1$ . The step-size is  $\delta\tau = 1/15$  and the trajectory length is 1 in all cases. The average is always consistent with one as required by reversibility.

| $N_{\text{smear}}$ | acc. rate | No. of traj | refl. | refr. | Mxv/traj.        |
|--------------------|-----------|-------------|-------|-------|------------------|
| 0                  | 69%       | 16          | 49    | 0     | $3.3 \cdot 10^5$ |
| 1                  | 66%       | 101         | 303   | 13    | $1.6 \cdot 10^5$ |
| 2                  | 93%       | 591         | 676   | 14    | $3.5 \cdot 10^4$ |

TABLE I: We give relevant quantities for the performance of the HMC algorithm for different levels of stout smearing. The data is take at  $\beta = 7.2$  and  $am_q = 0.05$ . We list the number of stout steps, the acceptance rate, the number of trajectories and the number of reflections and refractions during these trajectories. The last column gives the average number of applications of the kernel operator on a vector per trajectory.

The stout link  $\tilde{U}$  for one level of isotropic smearing is constructed from the gauge links by

$$\tilde{U}_\mu(x) = \exp(iQ_\mu)U_\mu(x) ; Q_\mu(x) = \left[ \frac{\rho}{i} V_\mu(x) U_\mu^+(x) \right]_{TH} \quad (31)$$

with  $V_\mu(x)$  the sum over all staples associated with the link and  $[\dots]_{TH}$  the traceless Hermitian part of the matrix. The contribution of this smearing to the fermion force has been worked out in Ref. [9].

A main effect of the smearing is to remove the majority of the eigenvalues of  $h(-R_0)$  close to 0. This has two effects. First, it implies that one has to compute fewer eigenvectors of the kernel operator to capture the ones within a certain distance to the origin. For the same number of inner eigenmodes the condition number of  $h^2$  is therefore smaller for the fat links than for thin links. This speeds up the inversion of the fermion Dirac operator. Furthermore, the computation of the fermion force is more stable since it is mainly plagued by small eigenmodes which are not well separated. This also implies a lower probability of two eigenmodes trying to change sign in the same HMC step, a problematic part of this algorithm. It furthermore might mean that the topology changes more rarely measured in HMC time and therefore lead to a higher auto-correlation time. However, it is not clear whether each of these attempts has the same probability of crossing over to the other topological sector or whether there is a correlation between consecutive attempts. This can only be clarified by an actual simulation.

To get an idea of the effect of this smearing, we started runs from an equilibrium configuration at  $\beta = 7.2$  and mass  $am_q = 0.05$  with  $\delta\tau = 1/20$ . We ran 16 trajectories with thin links, 101 with one level of stout smearing at  $\rho = 0.15$  and 591 with two levels of smearing. The plaquette is  $\langle \text{Tr}U_p \rangle \approx 1.67$  and the plaquette made of stout links is 2.5 for one level of stout links and 2.8 for two levels. In each of the runs we used two pseudo-fermion fields. The results of these runs are summarized in Table I. We find that each level of smearing reduces the cost per trajectory by roughly a factor of 3. The acceptance rate is the same for thin links and one level of smearing, however, it improves significantly for two levels. This is probably a result of the lower density of eigenmodes of the kernel action. The number of reflections and refractions per trajectory decreases with more levels of smearing. It is more than compensated for by the higher speed of the simulation.

Ref. [12] demonstrates that insufficient localization of the low-lying modes of the kernel operator  $h(-R_0)$  might

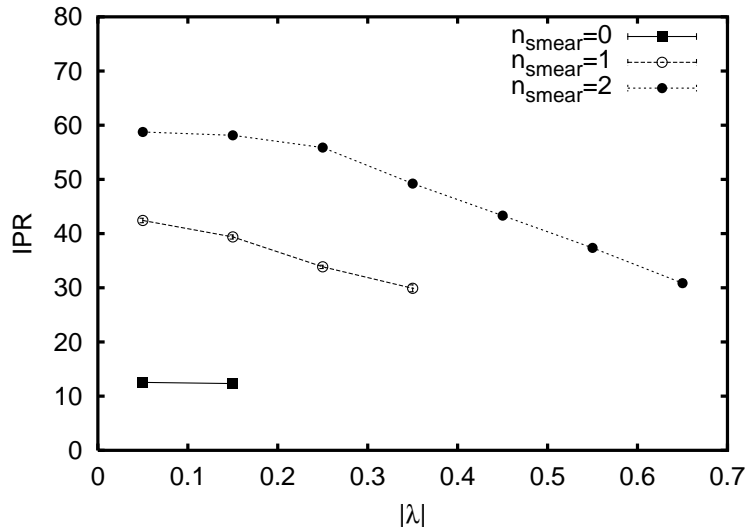


FIG. 6: The inverse participation ratio as a function of the modulus of the eigenvalue of  $h(-R_0)$ . The data is from the 8 lowest eigenmodes only and is binned in bins of size 0.1. It is taken from a run at  $\beta = 7.2$ ,  $am = 0.05$ . The modes of the Dirac operator constructed from thin links ( $n_{\text{smear}} = 0$ ) are only weakly localized (small IPR). Each smearing step increases the localization of the modes. The spectrum of  $h(-R_0)$  is denser near 0 for fewer smearing steps. Without smearing, we do not observe eigenvalues larger than 0.18 among the 8 lowest modes.

have implications on the locality of the overlap operator. We can get a rough measurement of the localization of the modes through the inverse participation ratio ( $V$  is the lattice volume)

$$I = V \sum_x [\psi^+(x)\psi(x)]^2. \quad (32)$$

If a mode is localized on a fraction  $f$  of the lattice volume, we expect  $I = 1/f$ . Fig. 6 shows a comparison of  $I$  from a set of simulations at  $\beta = 7.2$ ,  $am = 0.05$ , with either one or two levels of  $\rho = 0.15$  stout smearing, or simulations with a thin link. The inverse participation ratio (IPR) for the lowest eight modes has been binned and averaged. We immediately see that eigenmodes of  $h(-R_0)$  become progressively more localized with increasing smearing. The thin link kernel eigenmodes are large on about ten per cent of the lattice volume. This falls precipitously with smearing, to about two per cent for two smearing steps. We conclude that simulations with thin links at this set of parameter values are not only expensive, they are dangerously close to delocalization. (We are well aware, that we are comparing actions with different bare parameters in the fermion sector.) Since the lattice spacing for different fermion actions (due to different levels of smearing) might be different, we also computed the eigenmodes of the thin link  $h(-R_0)$  operator on the configurations from the fat link data set. We found essentially no difference to the IPR from the thin link data set.

We also notice that the range of eigenvalue of the lowest eight modes is considerably compressed as smearing is removed. This means that the range of the Zolotarev approximation of the step function must be increased, with a consequent increase in its evaluation cost due to the increased ill-conditioning of  $h^2 + c_i$ .

## V. CHANGING THE TOPOLOGICAL SECTOR

When running with only one pseudo-fermion field we found it very difficult to change topological sector, i.e. the algorithm reflected most of the time at the boundary. We observed that the height of the step was typically  $\mathcal{O}(200)$  compared to  $|\langle N, \pi \rangle|^2$  which is  $\mathcal{O}(1)$ . This is the case independent of the direction of the change in topology, e.g. whether one changes from  $Q = 0$  to  $Q = 1$  or vice versa. It only occurs rarely that  $\Delta S$  is such that a change in topology is possible and one gets long sequences without a change in topology indicating a high auto-correlation time.

Why is this so? The  $\phi$  field in the HMC algorithm with one pseudo-fermion field is generated with the distribution  $\exp(-\phi^+ H^{-2} \phi)$ . This is done by generating a Gaussian random vector  $R$  and then multiplying it by  $H$ . The expression which gives the contribution of the fermionic determinant during the evolution is thus given by  $\exp(-|H_1^{-1} H_0 R|^2)$  with  $H_0$  the Hermitian Dirac operator at the beginning of the trajectory and  $H_1$  the 'current' Hermitian Dirac operator. In Ref. [33] it was found that this is a good estimator for the change in the fermionic determinant only if the eigenvalues

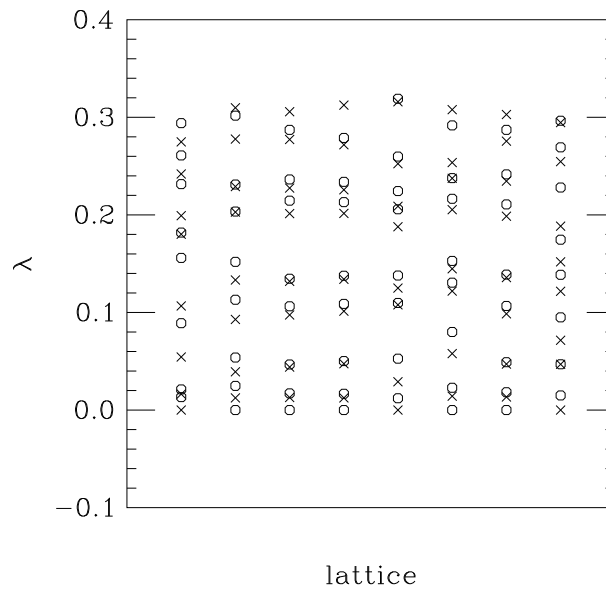


FIG. 7: Low-lying spectrum of  $H(0)^2$  for a set of  $\beta = 7.3$ ,  $m = 0.1$  lattices on either side of a topology-changing boundary. Octagons and crosses show the spectrum on either side.

of  $H_0$  and  $H_1$  are very similar. This is likely the case as long as one stays in the same topological sector. However, the eigenvalue spectrum changes significantly when the topological sector changes, e.g. two eigenvalues of  $H$ ,  $\pm\lambda$ , are transformed to  $\{m, 2R_0\}$  or vice versa. To be precise, the change in the determinants is given by

$$\frac{\det H_1^+ H_1}{\det H_0^+ H_0} \propto \int dR dR^+ e^{-R^+ R} e^{-R^+ \Omega R} . \quad (33)$$

with  $\Omega = H_0^+ H^{-2} H_0 - 1$ . The exponential function is bounded by zero from below. So large fluctuations in  $f[R] = \exp(-R^+ \Omega R)$  mean lots of events with  $f[R] \approx 0$  and only very few ones with  $f[R]$  large. For  $R^+ \Omega R$  this means a large number of (very) large values and only very few small ones. Small fluctuations, however, mean that  $R^+ \Omega R$  has values in a small interval around some constant given by the determinant ratio.

Thus, while  $H_1$  is in the same chiral sector as  $H_0$ , the change in the fermionic action is small. However, when we cross to the other chiral sector, the large fluctuations in the estimator are most likely such that  $\Delta S_f$  is a large number, which means that the trajectory will reflect from the boundary and stay in the same topological sector. It is therefore pivotal to employ a better estimator for the change in the determinant.

As an illustration of the change in the spectrum, we have computed a set of low-lying eigenmodes of  $H(0)^2$  on either side of a topology change. Specifically, we move onto the critical surface and compute the spectrum of  $H(0)^2$  twice, once with the eigenvalue of the lowest eigenmode set to its value just before the crossing, and then a second time with its eigenvalue's sign flipped. The parameters are  $\beta = 7.3$ ,  $m = 0.1$ . Fig. 7 shows that not only does a zero mode appear or disappear, but all the low lying eigenvalues of  $H(0)^2$  change discontinuously. This is to be expected: eigenmodes of Hermitian matrices repel, and the appearance of a zero mode (for example) must push nearby modes away.

To reduce fluctuations, we decided to use the method proposed in Refs. [14, 15], which consists of rewriting the fermion determinant as in Eq. (10). In this method, only determinant ratios are evaluated using pseudo-fermions for the light quark masses. The change in the spectra while changing topological sector of the ratio  $H(m)/H(m')$  can be expected to be less dramatic than the change of the spectrum of  $H(m)$ . Only the determinant of  $H(m_N)$  is evaluated directly. However, for a large mass  $m_N$  the spectrum of  $H^2$  is confined to a smaller region between  $m_N^2$  and  $4R_0^2$  and the change in the spectrum therefore less drastic than for a smaller mass. In order to distribute the contribution to the fermionic action equally among the different pseudo-fermion fields we choose the  $(N - 1)$  auxiliary masses for a sea quark mass of  $m_1$  to be

$$m_i = m_1^{(N-i+1)/N} . \quad (34)$$

In Fig. 8 we show the distribution of  $2\Delta S_f$  and  $|\langle N, \pi \rangle|^2$ . The topological sector changes if  $2\Delta S_f < |\langle N, \pi \rangle|^2$ . The data is taken from a run at  $\beta = 7.2$  and  $am_q = 0.05$  and  $\delta\tau = 1/20$ . We see that for the standard HMC with one

| No. of PF | trajectories | attempts/traj. | refr. prob. | MatVec / traj.      | acc. rate |
|-----------|--------------|----------------|-------------|---------------------|-----------|
| 1         | 602          | 1.3(1)         | 0.5(3)%     | $2.3(1) \cdot 10^5$ | 90%       |
| 2         | 591          | 1.2(1)         | 2.0(6)%     | $3.4(1) \cdot 10^5$ | 93%       |
| 3         | 290          | 1.6(2)         | 3(1)%       | $5.5(4) \cdot 10^5$ | 89%       |

TABLE II: The effect of additional pseudo-fermion fields. We list the the number of trajectories we analyzed, the attempts to change topology (reflections plus refractions) per trajectory, the percentage of refractions and the number of applications of  $h(-R_0)$  on a vector per trajectory. In the last column we give the acceptance rate. The data is taken at  $\beta = 7.2$  and  $am = 0.05$ .

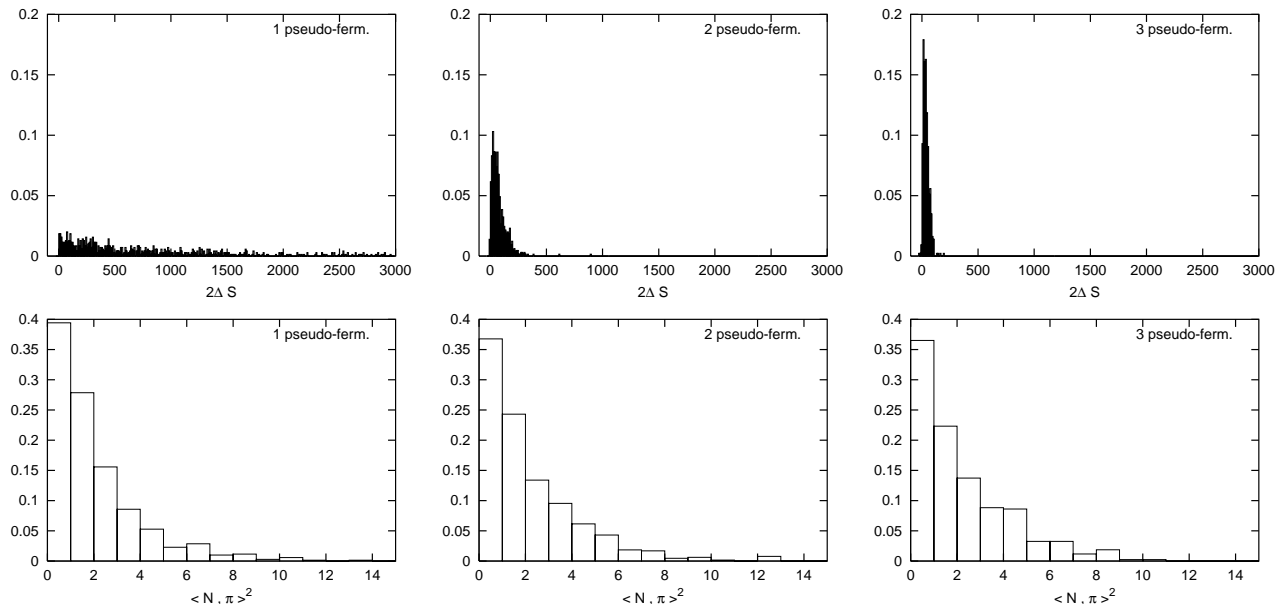


FIG. 8: Distribution of the two components which determine whether a trajectory reflects or refracts at the boundary between two topological sectors. Refraction takes place if  $2\Delta S < |\langle N, H \rangle|^2$ . The data is taken at  $\beta = 7.2$  and  $am_q = 0.05$ . For the 1 pseudo-fermion distribution of  $2\Delta S$  we do not show about 5% of the data which is above 3000.

pseudo-fermion field the distribution of  $2\Delta S_f$  is spread out up to values of several thousand whereas the distribution of  $|\langle N, \pi \rangle|^2$  only spreads up to  $\approx 10$ . (The distribution of  $|\langle N, \pi \rangle|^2$  is independent of the number of pseudo-fermion fields.) The spread of  $2\Delta S_f$  shrinks considerably with more pseudo-fermion fields.

In these runs we observed roughly 1.5 attempts per trajectory to cross over to another topological sector independent of the number of pseudo-fermion fields. (For a summary of the results see Table II.) The additional fields have a significant impact on the rate of topology changes. Whereas a change only occurs once in roughly 200 trajectories for one pseudo-fermion field, it occurs once per 35 trajectories for three pseudo-fermions. However, the additional fields seem to have no impact on the acceptance rate. The additional cost of the auxiliary fields is thus only justified by the higher tunneling rate and does not pay back in a possibility to decrease the step size as in the case of simulations with Wilson fermions. It appears from Table II that a single additional set of pseudofermions is sufficient.

In Fig. 9 we show the time history of the topological charge as a function of simulation time for three values of  $\beta$  and  $am_q = 0.1$ . The runs were done with three pseudo-fermion fields. Below the phase transition we observe a lot of changes in topology and  $|Q|$  up to 2. This is as expected since chiral symmetry is expected to be broken and the lattice spacing is large. With larger  $\beta$  the lattice spacing gets smaller, the temperature gets larger and we therefore expect fewer instantons and a smaller topological charge. This is confirmed by our simulations.

## VI. CONCLUSIONS

Simulations with two flavors of light dynamical overlap fermions with lattice spacing near  $a \simeq 1/(6T_c)$  and  $am_q = 0.05$  ( $m \simeq 50$  MeV?) and small volume (a few  $\text{fm}^4$ ) are certainly feasible on arrays of contemporary (2004) work stations. The crucial ingredient needed to do such simulations is a fermion action with a fat link gauge connection.

To be definite, we summarize our action: The gauge action is given by Eq. (28) with  $u_0 = 0.86$ . The kernel action

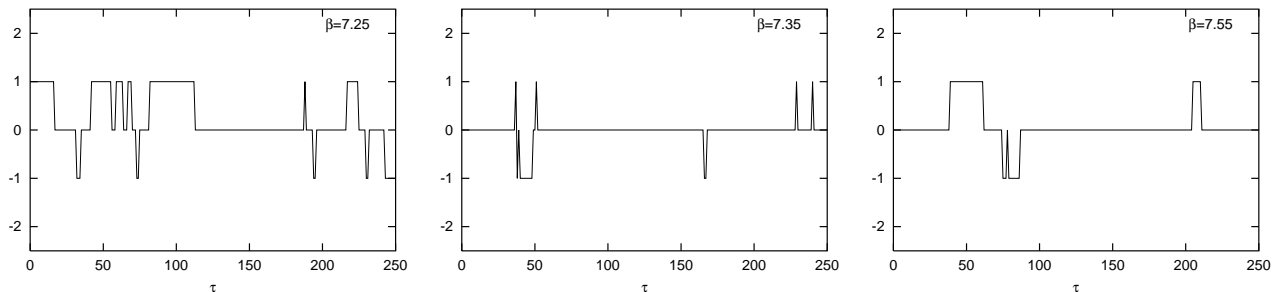


FIG. 9: The history of the topological charge in simulation time for  $am_q = 0.1$  at three values of  $\beta$ .  $\beta = 7.25$  is probably below the phase transition whereas  $\beta = 7.55$  is above. The runs were done with three pseudo-fermion fields.

is that of Eq. 8 with  $\rho_1 = -1/6$ ,  $\rho_2 = -1/18$ , a clover term with coefficient  $C_{SW} = 1.278$ , and the gauge connection is a two-level stout link with smearing parameter  $\rho = 0.15$ . We use it in the overlap with (negative) mass shift  $R_0 = 1.2$ .

We are quite aware, that we have not completely characterized how much more efficient fat link overlap actions are, than the conventional thin link ones. Table I suggests a factor of 10 at equal  $\delta\tau$  and a (probably a factor of 2) smaller  $\delta\tau$  is needed for equivalent acceptance rate. Suffice it to say, thin link overlap is so expensive that we could not do anything useful with it with our available resources. Observations such as Fig. 6 suggest that thin link overlap might require a smaller lattice spacing than  $a \simeq 1/(6T_c)$  to avoid delocalized kernel eigenmodes.

The use of additional pseudo-fermion fields as suggested by Hasenbusch is very beneficial to the rate at which the topological sector changes. However, at our parameter values it seems to have no impact on the HMC acceptance rate.

Conventional large-lattice simulations are of course still not possible with these actions with small computer resources, but there are physics issues whose solution is much more sensitive to exact chiral symmetry than to large volume. We hope to address them in the near future.

### Acknowledgments

This work was supported by the US Department of Energy. We are grateful to Z. Fodor and A. Hasenfratz for conversations and correspondence. Simulations were performed on the University of Colorado Beowulf cluster. We are grateful to D. Johnson for its construction and maintenance, and to D. Holmgren for advice about its design.

- 
- [1] H. Neuberger, Phys. Lett. B **417**, 141 (1998) [arXiv:hep-lat/9707022].
  - [2] H. Neuberger, Phys. Rev. Lett. **81**, 4060 (1998) [arXiv:hep-lat/9806025].
  - [3] Y. Aoki *et al.*, arXiv:hep-lat/0411006.
  - [4] M. Golterman and Y. Shamir, arXiv:hep-lat/0411007.
  - [5] A. Bode, U. M. Heller, R. G. Edwards and R. Narayanan, arXiv:hep-lat/9912043.
  - [6] Z. Fodor, S. D. Katz and K. K. Szabo, JHEP **0408**, 003 (2004) [arXiv:hep-lat/0311010].
  - [7] N. Cundy, S. Krieg, A. Frommer, T. Lippert and K. Schilling, arXiv:hep-lat/0409029.
  - [8] S. A. Gottlieb, W. Liu, D. Toussaint, R. L. Renken and R. L. Sugar, Phys. Rev. D **35**, 2531 (1987).
  - [9] C. Morningstar and M. J. Peardon, Phys. Rev. D **69**, 054501 (2004) [arXiv:hep-lat/0311018].
  - [10] T. DeGrand [MILC collaboration], Phys. Rev. D **63**, 034503 (2001) [arXiv:hep-lat/0007046].
  - [11] T. DeGrand, A. Hasenfratz and T. G. Kovacs, Phys. Rev. D **67**, 054501 (2003) [arXiv:hep-lat/0211006].
  - [12] M. Golterman and Y. Shamir, Phys. Rev. D **68**, 074501 (2003) [arXiv:hep-lat/0306002].
  - [13] J. C. Sexton and D. H. Weingarten, Nucl. Phys. B **380**, 665 (1992).
  - [14] M. Hasenbusch, Phys. Lett. B **519**, 177 (2001) [arXiv:hep-lat/0107019].
  - [15] M. Hasenbusch and K. Jansen, Nucl. Phys. B **659**, 299 (2003) [arXiv:hep-lat/0211042].
  - [16] P. H. Ginsparg and K. G. Wilson, Phys. Rev. D **25**, 2649 (1982).
  - [17] N. I. Akhiezer, Theory of approximation, F. Unger Pub. Co., New York, 1956.
  - [18] N. I. Akhiezer, Elements of the theory of elliptic functions, American Mathematical Society, Providence, R.I., 1990.
  - [19] Cf. B. Jegerlehner, Nucl. Phys. (Proc. Suppl.) **63**, 958 (1998), hep-lat/9612014; A. Frommer, B. Nockel, S. Güsken, T. Lippert and K. Schilling, Int. J. Mod. Phys. C6, 627 (1995) [hep-lat/9504020].
  - [20] T. Kalkreuter and H. Simma, Comput. Phys. Commun. **93**, 33 (1996) [arXiv:hep-lat/9507023].
  - [21] N. Cundy, J. van den Eshof, A. Frommer, S. Krieg, T. Lippert and K. Schafer, arXiv:hep-lat/0405003.

- [22] C. Gattringer, I. Hip and C. B. Lang, Nucl. Phys. B **597**, 451 (2001) [arXiv:hep-lat/0007042].
- [23] P. Hasenfratz, S. Hauswirth, K. Holland, T. Jörg, F. Niedermayer and U. Wenger, Int. J. Mod. Phys. C **12**, 691 (2001) [arXiv:hep-lat/0003013].
- [24] C. Gattringer *et al.* [BGR Collaboration], Nucl. Phys. B **677**, 3 (2004) [arXiv:hep-lat/0307013].
- [25] R. Narayanan and H. Neuberger, Phys. Rev. D **62**, 074504 (2000) [arXiv:hep-lat/0005004].
- [26] W. H. Press, S. A. Teukolsky, W. T. Vetterling, B. P. Flannery, Numerical Recipes in C: The Art of Scientific Computing, 2nd ed., Cambridge University Press, New York, 1992
- [27] M. Lüscher and P. Weisz, Commun. Math. Phys. **97**, 59 (1985) [Erratum-ibid. **98**, 433 (1985)].
- [28] M. G. Alford, W. Dimm, G. P. Lepage, G. Hockney and P. B. Mackenzie, Phys. Lett. B **361**, 87 (1995) [arXiv:hep-lat/9507010].
- [29] A. Hasenfratz and F. Knechtli, Phys. Rev. D **64**, 034504 (2001) [arXiv:hep-lat/0103029].
- [30] See <http://physics.indiana.edu/~sg/milc.html>.
- [31] M. Lüscher, Nucl. Phys. Proc. Suppl. **106**, 21 (2002) [arXiv:hep-lat/0110007].
- [32] T. G. Kovacs, Phys. Rev. D **67**, 094501 (2003) [arXiv:hep-lat/0209125].
- [33] A. Hasenfratz and A. Alexandru, Phys. Rev. D **65**, 114506 (2002) [arXiv:hep-lat/0203026].